



Article

Tourmaline as a petrogenetic indicator highlighted in a multicoloured crystal from the gem deposit of Mavuco, Alto Ligoña pegmatite district, NE Mozambique

Mineralogy, petrology and geochemistry of pegmatites: Alessandro Guastoni memorial issue

Alessandra Altieri¹ , Federico Pezzotta² , Henrik Skogby³, Ulf Hålenius³ and Ferdinando Bosi^{1,4}

¹Department of Earth Sciences, Sapienza University of Rome, Piazzale Aldo Moro 5, I-00185 Rome, Italy; ²MUM – Mineralogical Museum “Luigi Celleri”, San Piero in Campo, Elba Island, Italy; ³Department of Geosciences, Swedish Museum of Natural History, Box 50007, SE-10405 Stockholm, Sweden; and ⁴CNR-IGAG c/o Department of Earth Sciences, Sapienza University of Rome, Italy

Abstract

A rounded fragment of a multicoloured tourmaline crystal (2.5 cm diameter), collected from the secondary gem deposit of Mavuco, Alto Ligoña pegmatite district, Mozambique, has been investigated using a multi-analytical approach, with the objective of reconstructing its growth history. The sample represents a core-to-rim section, perpendicular to the *c* axis, of a crystal characterised by a variety of colours. These change from a black core to an intermediate zone with a series of colours, yellow, blue–green and purple, to a final dark-green prismatic overgrowth. These changes are the result of a wide variation in Fe, Mn, Ti and Cu concentrations and their redox state. The black core is characterised by enrichment in Fe and Mn, with iron present in its divalent state. The yellow zone shows a progressive depletion in Fe and its colouration is caused by Mn²⁺ and Mn²⁺-Ti⁴⁺ IVCT interactions. The progressive decrease in Mn coupled with the absence of Ti, and the lack of Fe, implies that Cu²⁺ acts as the only chromophore in the pale blue–green zone. The dominant colour-causing agent of the purplish zone is Mn³⁺, denoting a change in redox environment; however, even though the amount of Cu remains significant, its chromophore effect is obscured by Mn³⁺. The dark-green prismatic overgrowth, characterised by a sharp increase in Fe, Mn and also Ca, is interpreted as a late-stage partial re-opening of the geochemical system. This occurrence could potentially be related to mechanical instability of the cavity in which the crystal grew.

Keywords: tourmaline-supergrupp minerals; petrogenetic indicator; growth history; gem tourmaline; Paraiba tourmaline; Cu-rich tourmaline; electron microprobe; optical absorption spectroscopy; Mössbauer spectroscopy

(Received 11 February 2024; accepted 10 May 2024; Accepted Manuscript published online: 20 May 2024)

Introduction

Tourmaline is the dominant host for boron in most rocks of the Earth's crust. It occurs in granites and granitic pegmatites, and also in sedimentary and in low-grade to ultrahigh-pressure metamorphic rocks and as detrital grains in sandstones and conglomerates (Ertl *et al.*, 2010; van Hinsberg *et al.*, 2011a, 2011b; Dutrow and Henry, 2018; Henry and Dutrow, 2018). Tourmaline-supergrupp minerals are complex borosilicates with a significant compositional variability containing both light and heavy elements, from H to Pb, and across multiple valence states.

This variability results in a wide range of distinct mineral species. The general structural formula of the tourmaline-supergrupp minerals is $XY_3Z_6T_6O_{18}(BO_3)_3V_3W$, where X = Na, K, Ca, Pb and □ (□ = vacancy); Y = Al, Fe³⁺, Mn³⁺, Cr, V, Mg, Fe²⁺, Mn²⁺, Li and Ti; Z = Al, Fe, Cr, V, Mg and Fe²⁺; T = Si, Al and B; B = B³⁺; V = (OH) and O; and W = (OH), F and O (Henry *et al.*, 2011). The non-italicised letters X, Y, Z, T and B represent groups of cations accommodated at the ^[9]X, ^[6]Y, ^[6]Z, ^[4]T and ^[3]B crystallographic sites (italicised letters). The letters V and W represent groups of anions accommodated at the ^[3]O(3) and ^[3]O(1) crystallographic sites, respectively. The H atoms occupy the H(3) and H(1) sites, which are related to O(3) and O(1), respectively.

According to the dominance of specific ions at one or more sites of the crystal structure, the tourmaline-supergrupp minerals can be classified in three primary groups on the basis of the X-site occupancy: X-site vacant, alkali and calcic (Henry *et al.*, 2011). A further level of classification into subgroups is based on charge arrangements at the Y and Z sites. Tourmalines are also

Corresponding author: Alessandra Altieri; Email: alessandra.altieri@uniroma1.it

Guest Editor: Fabrizio Nestola

This paper is part of a thematic set on pegmatites in memory of Alessandro Guastoni

Cite this article: Altieri A., Pezzotta F., Skogby H., Hålenius U. and Bosi F. (2024)

Tourmaline as a petrogenetic indicator highlighted in a multicoloured crystal from the gem deposit of Mavuco, Alto Ligoña pegmatite district, NE Mozambique. *Mineralogical Magazine* 88, 745–754. <https://doi.org/10.1180/mgm.2024.42>

distinguished by the dominant W anion into hydroxy-, fluor- and oxy-species (Henry *et al.*, 2011). In particular, occupancy of the X and Y-site is useful to reconstruct the chemical history of the fluids involved in tourmaline crystallisation (van Hinsberg *et al.*, 2011a, 2011b; Dutrow and Henry, 2018; Bosi *et al.*, 2022; Altieri *et al.*, 2022; 2023a, 2023b).

Tourmaline is well known to be an efficient geological tool for investigating P - T - X conditions in all crustal settings within the Earth given its ability to register and preserve the composition and the redox conditions of the environment from which it crystallised (Dutrow and Henry, 2011). Colour-zoning in tourmaline generally highlights internal variations in composition, reflecting evolution in the physico-chemical characteristics of the pegmatitic fluid during crystallisation (e.g. Dutrow and Henry, 2018; Altieri *et al.*, 2022; 2023a, 2023b).

The Mavuco tourmaline gem deposit, located in the Alto Ligoña pegmatite district (NE Mozambique), is internationally known to be the source of a quantity of very valuable Cu-bearing gem tourmalines also known as ‘Paraiba’ variety (Laurs *et al.*, 2008; Ertl *et al.*, 2013; Okrusch *et al.*, 2016). Nevertheless, as the deposit is of secondary origin, very little is known about the original primary deposit in which the tourmalines formed. To investigate the nature of the primary deposit and eventual changes in the crystallisation environment, and consequently, reconstruct the tourmaline growth history, a tourmaline sample comprising a large fragment of a multicolour crystal has been chosen that gives the best representation of the variety of colours occurring in the deposit. This multicoloured sample has been subject to an in-depth analysis using a multi-analytical approach, including electron microprobe analysis, optical absorption and Mössbauer spectroscopic investigations.

Sample occurrence

The mining area of Mavuco consists of a secondary deposit of over 12 km² located in the Alto Ligoña pegmatite district, in NE Mozambique (Fig. 1a). In this secondary deposit, tourmalines occur as fragments, ranging usually from 1 g to over 100 g with

sub-angular to sub-rounded morphology, within a residual soil level mostly composed of quartz fragments and associated occasionally with fragments of gem beryl and spessartine. This layer is called *kamada* by local miners, with a thickness ranging from a few cm up to 1 m, and occurs on top of the altered bedrock, which is, in general, composed of amphibolitic paragneiss, and more rarely of marble lenses, and aplitic and pegmatitic veins. On top of the *kamada* is a layer named locally as *kororo*, a reddish-brownish soil unit with a thickness from 1 m up to exceptionally over 10 m. This layer is bauxitic with variable quantities of iron hydroxide nodules and sparse small quartz grains. Tourmaline or other gemstones are not present in this layer.

This secondary gem deposit was interpreted by Laurs *et al.* (2008) (Fig. 1b) as of alluvial origin, with the primary pegmatitic tourmaline deposits eroded and transported by the seasonal streams through spasmodic flash floods downhill to the Mavuco area where they were deposited (Laurs *et al.*, 2008). Nevertheless, systematic observations made by one of the authors (Pezzotta) of the soil sections exposed during the mechanised excavations for the mining of gem tourmalines, performed by the Mozambique Gems company, show that the distribution and the thickness of the *kamada* are not related to the morphology and hydrology of the land, and indeed the *kamada* represents a very persistent unit in the soil, occurring at various depths from place to place, though always at the top of the altered bedrock. Moreover, the occurrence in the *kamada* of quartz and tourmaline clasts, and occasionally beryl and spessartine clasts, which still preserve quite well-defined crystal faces, together with clasts which are partially rounded to very rounded, and the local increase of the *kamada* thickness at the intersection and in the surrounding areas of altered quartz and pegmatitic veins still observable in the altered bedrock, are elements in favour of an eluvial, and locally colluvial, origin of such a soil unit. Thus, the minerals found as fragments in the *kamada* are the result of an *in situ* erosion of a primary deposit, composed, very probably, of a series of pegmatitic veins, which, at least in part, still exist at depth. Further studies are in progress by Pezzotta to define better this genetic model.

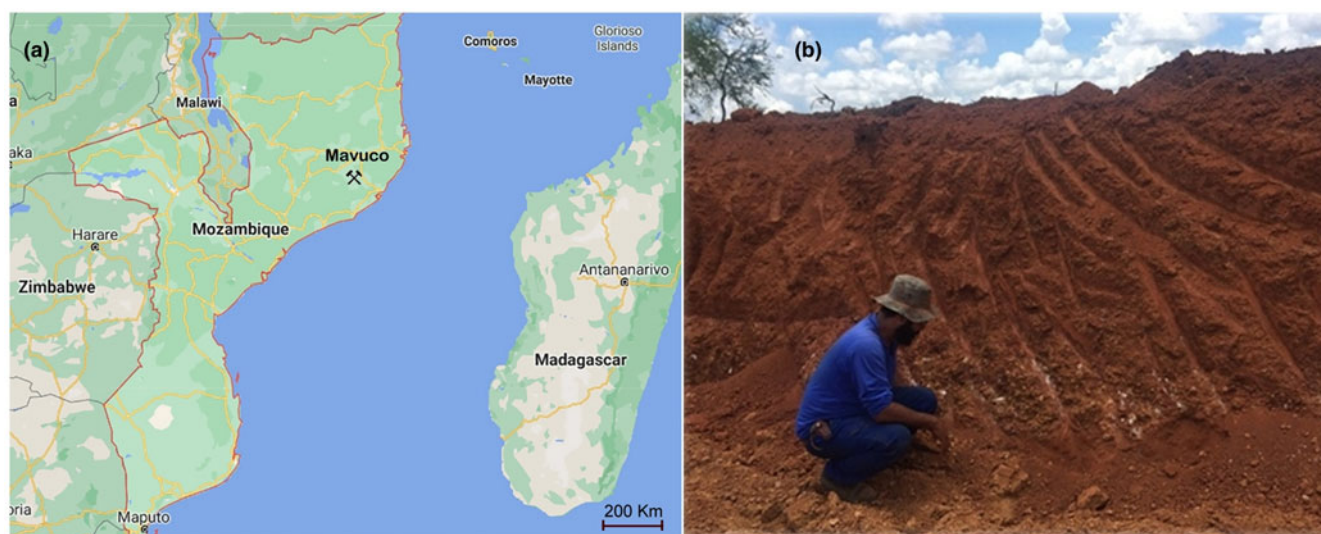


Figure 1. (a) The occurrence area of the tourmaline sample investigated is marked in the eastern portion of the Pegmatitic District of Alto Ligoña, NE Mozambique; and (b) a cross-section of the soil of the secondary deposit of Mavuco. Tourmalines are found in a light reddish-brown quartz-rich gravel layer (locally called *kamada*) on top of a light tan weathered bedrock, and underneath a layer of red-brown clayey-bauxitic soil (locally called *kororo*). Photo by F. Pezzotta.

Materials and methods

Sample

A sample (labelled 'MAV 6') consisting of a large fragment (2.5 cm diameter, 12.75 g weight) of a multicoloured tourmaline crystal collected from the secondary deposit of Mavuco, roughly representative of a core-to-rim section perpendicular to the *c* axis, was chosen for the present study (Fig. 2, left). The sample is sub-rounded and results from the natural breakage and erosion of an original prismatic crystal, characterised by a black core, an intermediate polychromatic zone (yellow, pale blue-green, purple) and a dark-coloured rim.

On the basis of the compositional and colour inhomogeneity, the sample was divided in different zones. The area corresponding to the core zone, the intermediate polychromatic zone and the dark-green prismatic rim were labelled 'C', 'I' and 'R', respectively. The 'I' and 'C' zones were further subdivided, on the basis of changes in composition or colour, by adding a progressive numerical suffix starting from the core of the crystal.

Sample preparation

The tourmaline sample was glued to a glass slide using epoxy resin. Then, a crystal slice was cut and subsequently ground and polished to produce a flat surface with a uniform thickness of 500 μm for compositional microanalysis (Fig. 2, right).

For optical absorption spectroscopy analysis, crystal slices cut from the different coloured zones were glued to a glass slide using a thermoplastic resin. Before analysis, each coloured slice was further thinned to appropriate thickness (yellow intermediate zone: 280 μm ; pale blue-green intermediate zone: 838 μm ; purple intermediate zone: 843 μm ; dark-green rim: 424 μm) and doubly polished.

Electron microprobe analysis (EMPA)

Compositional data for the tourmaline sample were collected along a straight line traverse from the black core to the dark-green

rim with an average step size of 500 μm , using a CAMECA SX50 electron-microprobe at the Istituto di Geologia Ambientale e Geoingegneria (CNR of Rome, Italy). Forty four spot analyses were obtained. Electron microprobe analyses were obtained in wavelength-dispersion spectroscopy mode with an accelerating potential of 15 kV, a sample current of 15 nA and a beam diameter of 10 μm . Minerals and synthetic compounds used as reference materials were: wollastonite (Si, Ca), magnetite (Fe), rutile (Ti), corundum (Al), karelianite (V), fluorophlogopite (F), periclase (Mg), jadeite (Na), orthoclase (K), rhodonite (Mn) and metallic Cr, Cu and Zn. The PAP correction procedure for quantitative electron microprobe analysis was applied (Pouchou and Pichoir, 1991). Relative error for these data was <1% and detection limits <0.03 wt.%.

Mössbauer spectroscopy (MS)

^{57}Fe Mössbauer spectra of the Fe-rich coloured zones of the tourmaline sample were collected using a conventional spectrometer system equipped with a 50 mCi source and operated in constant acceleration mode. The absorbers were prepared from 60 to 135 mg ground sample material that was mixed with an acrylic resin and pressed to 12 mm diameter discs under mild heating (<150°C). Data were collected at room temperature over the velocity range ± 4.2 mm/s and recorded in a multichannel analyser with 1024 channels. The velocity was calibrated with an α -Fe foil. The spectra were fitted using unconstrained Lorentzian doublets with the aid of the software *MossA* (Prescher *et al.*, 2012).

Optical absorption spectroscopy (OAS)

Unpolarised, room-temperature optical absorption spectra of the polychromatic core zone and the dark-green rim, in the range of 30500–11000 cm^{-1} , were obtained at a spectral resolution of 1 nm on doubly polished sections, using an AVASPEC-ULS2048 \times 16 spectrometer attached via a 400 μm ultraviolet (UV) optical fibre cable to a Zeiss Axiotron UV-microscope. A 75 W Xenon

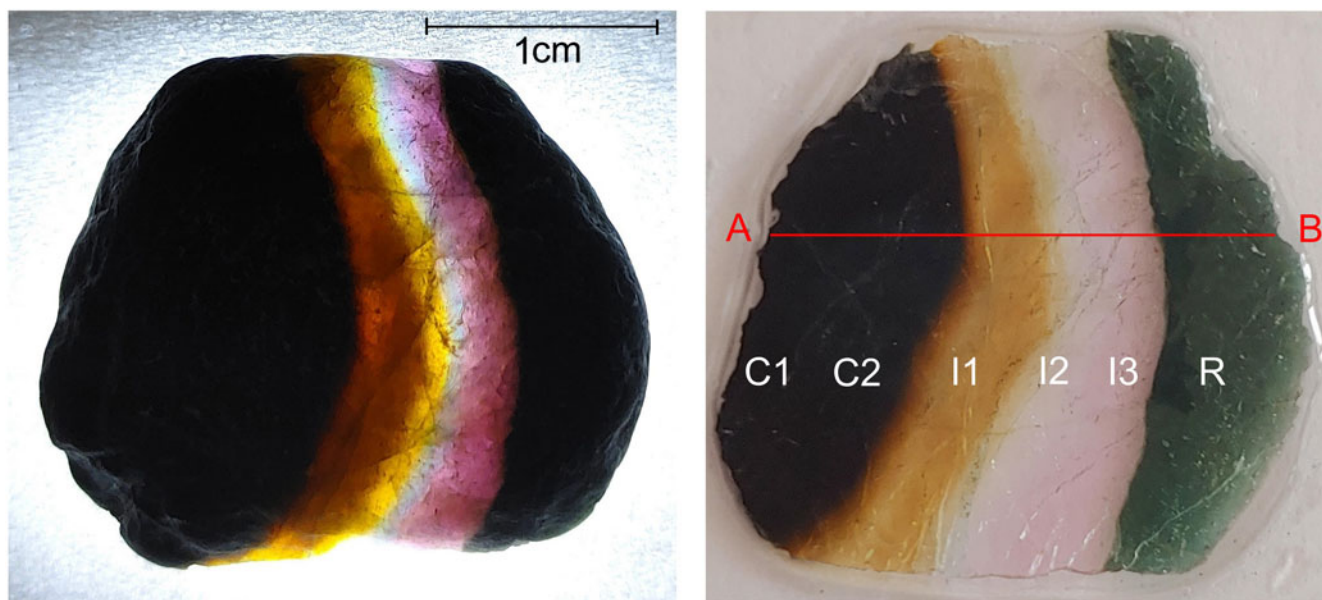


Figure 2. The polychromatic tourmaline sample investigated in this work (image to the left) and the corresponding thin (500 μm) section (image to the right). Sample size: 2.5 cm. Sample weight: 12.75 gr. Scale bar = 1 cm. The analysed traverse (A–B) is represented by a solid red line. On the basis of colour and composition, the different coloured zones are labelled as: C1, C2 = core zones; I1 = yellow intermediate zone, I2 = pale blue-green intermediate zone (note that the real colour of the crystal in the figure appears faded due to the backlighting) and I3 = pink-red intermediate zone; R = prismatic overgrowth.

arc lamp was used as light source and Zeiss Ultrafluor 10× lenses served as objective and condenser. Data in the NIR region (11000–5000 cm^{-1}) were measured using a Bruker Vertex 70 spectrometer attached to a Hyperion 2000 microscope and equipped with a halogen lamp source, a CaF_2 beamsplitter and an InSb detector at resolution of 4 cm^{-1} .

Determination of atomic fractions

The wt.% of element oxides determined by EMPA (Table 1) was used to calculate the atomic fractions (atoms per formula unit, apfu). The B content was assumed to be stoichiometric ($B = 3.00$ apfu). Lithium was calculated in accord with Pesquera *et al.* (2016). Iron oxidation state in the Fe-rich coloured zones was determined by MS (Table 2). The (OH) content was calculated by charge balance with the assumption of $(T + Y + Z) = 15.00$ apfu and 31 anions. The site populations and the empirical formulae (Table 3) of the different coloured zones of the tourmaline sample analysed were calculated following the site allocation of ions recommended by Henry *et al.* (2011).

Results

Composition

Electron microprobe analyses of the sample revealed a wide variation in Fe- and Mn- concentrations, reflected in marked changes in colour from the black core, to yellow, pale blue–green, purple in the intermediate zone, and to dark green at the prismatic overgrowth, representing the rim. Calcium, Ti, Cu and F are also characterised by some variation along the traverse. Vanadium, Cr and Zn were below detection limits.

The determined concentrations of selected elements (as wt.% oxides) along the chosen traverse are shown Fig. 3, and average compositions for each coloured zone summarised in Table 1.

The black core of the sample (C1 and C2) is characterised by enrichment in Fe and Mn ($\text{FeO} \approx 5$ wt.% and $\text{MnO} \approx 4$ wt.%), which remains quite constant throughout the section (Fig. 3). Within the intermediate polychromatic zone, the yellow zone (I1), there is a sharp increase in MnO, reaching up to 7 wt.%, coupled with a simultaneous drop in FeO to less than 1 wt.% (Fig. 3). A decrease in the MnO content occurs in the pale blue–

Table 1. Average compositions from EMPA and atoms per formula unit (apfu) for the different coloured zones of the tourmaline sample from the Mavuco area, Alto Ligoña pegmatite district, NE Mozambique.

	C1 <i>n</i> = 12	C2 <i>n</i> = 5	I1 <i>n</i> = 10	I2 <i>n</i> = 3	I3 <i>n</i> = 3	R <i>n</i> = 11
SiO_2 (wt.%)	37.16(27)	36.45(16)	37.55(54)	38.86(29)	39.64(2)	39.40(25)
TiO_2	0.45(2)	0.65(4)	0.45(9)	0.04(8)	0.02(2)	0.05(2)
B_2O_3^a	10.66	10.62	10.83	11.09	11.15	10.95
Al_2O_3	36.21(34)	37.16(56)	37.82(40)	39.99(47)	39.96(15)	36.57(23)
FeO	4.99(20)	3.95(75)	0.36(46)	0.02(1)	0.01(1)	1.39(26)
Fe_2O_3^c	0.09	–	–	–	–	0.06
MnO	4.27(13)	4.33(23)	6.23(76)	1.47(74)	0.06(11)	1.11(14)
Mn_2O_3^d	–	–	–	–	0.56	–
MgO	0.03(1)	0.01(1)	0.00(1)	0.01(1)	–	0.19(6)
CuO	0.04(3)	0.01(2)	0.06(5)	0.13(2)	–	0.03(3)
CaO	0.33(8)	0.63(7)	0.92(16)	1.53(5)	1.31(3)	4.03(23)
Na_2O	2.31(4)	2.32(5)	2.26(10)	1.64(4)	1.62(2)	0.95(15)
Li_2O^b	1.00	0.97	1.36	2.09	2.34	2.39
K_2O	0.03(1)	0.03(1)	0.02(1)	0.01(1)	0.02(1)	0.01(1)
F	0.82(12)	0.83(12)	1.18(15)	1.15(19)	1.14(11)	1.48(14)
H_2O^a	2.91	2.71	2.74	2.98	2.93	2.61
$-\text{O} \equiv \text{F}$	–0.35	–0.35	–0.50	–0.49	–0.48	–0.62
Total	100.92	100.35	101.29	100.53	100.32	100.51
Atoms normalised to 31 anions						
Si (apfu)	6.057	5.968	6.023	6.091	6.179	6.185
Ti^{4+}	0.055	0.079	0.054	0.005	0.002	0.006
B	3.000	3.000	3.000	3.000	3.000	3.000
Al	6.955	7.170	7.151	7.388	7.342	6.889
Fe^{2+}	0.669	0.541	0.048	0.002	0.001	0.175
Fe^{3+}	0.011	–	–	–	–	0.008
Mn^{2+}	0.590	0.600	0.846	0.196	0.008	0.147
Mn^{3+}	–	–	–	–	0.066	–
Mg	0.007	0.002	0.000	–	–	0.047
Cu	0.005	0.001	0.007	0.014	0.013	0.004
Ca	0.057	0.110	0.157	0.258	0.218	0.679
Na	0.731	0.738	0.702	0.498	0.491	0.289
Li	0.655	0.639	0.878	1.318	1.467	1.509
K	0.006	0.007	0.005	0.003	0.003	0.003
F	0.423	0.430	0.598	0.571	0.564	0.736
OH	3.170	2.965	2.930	3.118	3.042	3.264

^aCalculated by stoichiometry (see text)

^bEstimated with the procedure of Pesquera *et al.* (2016)

^cCalculated by Mössbauer analysis; for C1 and R, $\text{FeO}_{\text{EMPA}} = 4.99(20)$ wt.% and $\text{FeO}_{\text{EMPA}} = 1.39(26)$ wt.%, respectively

^dDetermined by OAS

Errors for oxides and fluorine are standard deviations (in brackets); ‘–’ is below detection limit

Table 2. Room temperature ^{57}Fe Mössbauer parameters for the FeO-rich coloured zones of the tourmaline investigated in this study.*

	δ (mm/s)	ΔE_Q (mm/s)	Γ (mm/s)	Assignment	%Area
Black core (C1, C2)	1.09	2.51	0.26	Fe^{2+} (Y1)	35
	1.09	2.30	0.28	Fe^{2+} (Y2)	37
	1.05	1.60	0.59	Fe^{2+} (Y3)	25
	0.70	1.07	0.47	$\text{Fe}^{2.5+}$	3
Yellow zone (I1)	1.08	2.41	0.32	Fe^{2+} (Y1)	68
	1.16	1.98	0.57	Fe^{2+} (Y2)	32
Dark-green overgrowth (R)	1.09	2.37	0.30	Fe^{2+} (Y1)	66
	1.09	2.59	0.25	Fe^{2+} (Y2)	21
	1.01	1.56	0.66	Fe^{2+} (Y3)	9
	0.60	0.71	0.50	Fe^{3+}	4

*Centroid shift (δ) in mm/s relative to α -Fe foil; errors are estimated no less than ± 0.02 mm/s for δ , quadrupole splitting (ΔE_Q), and peak width (Γ), and no less than $\pm 3\%$ for doublets areas.

green zone (I2), with a progressive decrease to below 1 wt.% approaching the termination of the purple zone (I3), similarly for FeO, which falls to values below the detection limits in the I3 zone (Fig. 3). The dark-green prismatic rim (R) is characterised by a sharp increase in FeO and a moderate increase in MnO concentration, reaching up to 1.4 and 1.2 wt.%, respectively (Fig. 3).

In addition to FeO and MnO, the concentrations of CuO, TiO₂ and CaO, show significant changes within the crystal. CuO concentration is above detection only in the yellow I1 zone, the pale blue-green I2 zone and the purple I3 zone, with values up to 0.15 wt.% (Fig. 3). Titanium is concentrated mostly in the C1, C2 and I1 zones, with values of TiO₂ ranging from 0.45 to 0.65 wt.%, though it is below 0.05 wt.% in the I2 and I3 zones and the dark-green prismatic overgrowth (Table 1). A peculiar behaviour is seen for CaO content, which though generally low across all the zones of the crystal, displays an abrupt increase in the R zone, reaching ~ 4 wt.% (Fig. 3).

Mössbauer spectroscopy data and iron speciation

Portions of the black core (C1, C2), the yellow intermediate zone (I1) and the dark-green prismatic overgrowth (R), characterised by significant Fe contents, were subjected to MS analysis to evaluate the Fe oxidation states. The hyperfine parameters of the MS doublets and the relative Fe oxidation state and site assignment for each sample analysed are summarised in Table 2. The spectrum of the black core zone was fitted with four doublets. The first three doublets are compatible with Fe^{2+} occurring at the Y site (Andreozzi *et al.*, 2008). However, a unique Fe site-distribution cannot be achieved due to the limited resolution of the absorption doublets. A fourth weak doublet (3.2%) was interpreted as $\text{Fe}^{2.5+}$ due to electron delocalisation. These data resulted in a $\text{Fe}^{3+}/\Sigma\text{Fe}_{\text{tot}}$ -ratio of 0.02 (with $\text{Fe}^{2.5+}$ distributed equally on

Fe^{2+} and Fe^{3+}), suggesting that Fe^{2+} strongly dominates the black core zone (Fig. 4a). The spectrum of the yellow intermediate zone was fitted with only Fe^{2+} doublets compatible with Y-site occupancy, without any indication of Fe^{3+} (Fig. 4b). For the dark-green overgrowth, a model with four absorption doublets was adopted. The first three doublets were interpreted as Fe^{2+} at the Y site (Y1, Y2 and Y3), whereas the fourth doublet is consistent with Fe^{3+} (4% of Fe_{tot}) (Fig. 4c).

Optical spectra

As stated above, the tourmaline sample is characterised by a marked polychroism. The different coloured zones were subjected to optical absorption spectroscopy analysis in the UV-Vis region with the spectra of the yellow, pale blue-green and purple intermediate zones and the dark-green prismatic overgrowth reported in Fig. 5.

The spectrum of the yellow intermediate zone (I1) has a very strong absorption band in the near UV-region at ~ 30700 cm^{-1} and a sharp and very weak absorption band at ~ 24000 cm^{-1} . The spectrum recorded in the pale blue-green intermediate zone (I2) reveals only the presence of a very weak broad band at ~ 14000 cm^{-1} and an intense broad band at ~ 11000 cm^{-1} in the near-infrared range (NIR). The recorded optical absorption spectrum of the purple intermediate zone (I3) is characterised by weak and broad absorption bands at ~ 25200 cm^{-1} , ~ 22000 cm^{-1} and ~ 14000 cm^{-1} , and a stronger broad band at ~ 19000 cm^{-1} . The spectrum of dark-green prismatic overgrowth displays two broad absorption bands centred at 13800 cm^{-1} and 9200 cm^{-1} , and a set of weak and relatively sharp bands between ~ 25000 – 24000 cm^{-1} .

The set of sharp bands, in the NIR region of spectra between 6700–7200 cm^{-1} , are due to overtones of the fundamental (OH)-stretching modes. These bands are obscured in the spectrum of the dark-green overgrowth by the strong absorption band at ~ 9000 cm^{-1} , and barely visible in the spectrum of the yellow intermediate zone (I1) due to the reduced thickness.

Classification of tourmaline species in the multicoloured crystal from the gem deposit of Mavuco, Alto Ligoña pegmatite district, Mozambique

The empirical formulae (Table 3) show that the composition of the black core zone (C1), as well as the yellow (I1), the pale blue-green (I2) and the purple (I3) intermediate zones, are consistent with a tourmaline belonging to the alkali-group, subgroup 2 (Henry *et al.*, 2011): they are Na-dominant at the X position of the tourmaline general formula and fluor-dominant at W with $(\text{OH}+\text{F})^- > \text{O}^{2-}$ and $\text{F} \gg (\text{OH})$. In addition, they are $^{\text{Z}}\text{Al}$ - and $^{\text{Y}}(\text{Al}_{1.5}\text{Li}_{1.5})$ -dominant. Thus, the black core zone (C1), the yellow (I1), the pale blue-green (I2) and the purple (I3) intermediate zones can be classified as fluor-elbaite, ideally $\text{Na}(\text{Li}_{1.5}\text{Al}_{1.5})\text{Al}_6\text{Si}_6\text{O}_{18}(\text{BO}_3)_3(\text{OH})_3\text{F}$.

Table 3. Empirical formulae for the different coloured zones of the tourmaline sample investigated.

Coloured zones	Empirical formulae
Black inner core (C1)	$^{\text{X}}(\text{Na}_{0.73}\text{K}_{0.01}\square_{0.21}\text{Ca}_{0.06})\Sigma_{1.00}^{\text{Y}}(\text{Al}_{0.96}\text{Li}_{0.66}\text{Fe}_{0.67}^{2+}\text{Fe}_{0.01}^{3+}\text{Mn}_{0.59}^{2+}\text{Mg}_{0.01}\text{Ti}_{0.06})\Sigma_{2.94}^{\text{Z}}\text{Al}_6(\text{Si}_{6.06}\text{O}_{18})(\text{BO}_3)_3^{\text{V}}(\text{OH})_{3.00}^{\text{W}}(\text{OH}_{0.17}\text{F}_{0.42}\text{O}_{0.41})\Sigma_{1.00}$
Black outer core (C2)	$^{\text{X}}(\text{Na}_{0.74}\text{K}_{0.01}\square_{0.14}\text{Ca}_{0.11})\Sigma_{1.00}^{\text{Y}}(\text{Al}_{1.14}\text{Li}_{0.64}\text{Fe}_{0.54}^{2+}\text{Mn}_{0.60}^{2+}\text{Ti}_{0.08})\Sigma_{3.00}^{\text{Z}}\text{Al}_6[(\text{Si}_{5.97}\text{Al}_{0.03})\text{O}_{18}](\text{BO}_3)_3^{\text{V}}(\text{OH}_{2.97}\text{O}_{0.03})\Sigma_{3.00}^{\text{W}}(\text{F}_{0.43}\text{O}_{0.57})\Sigma_{1.00}$
Yellow intermediate zone (I1)	$^{\text{X}}(\text{Na}_{0.70}\square_{0.14}\text{Ca}_{0.16})\Sigma_{1.00}^{\text{Y}}(\text{Al}_{1.15}\text{Li}_{0.88}\text{Fe}_{0.05}^{2+}\text{Mn}_{0.85}^{2+}\text{Cu}_{0.01}\text{Ti}_{0.05})\Sigma_{2.99}^{\text{Z}}\text{Al}_6(\text{Si}_{6.01}\text{O}_{18})(\text{BO}_3)_3^{\text{V}}(\text{OH}_{2.93}\text{O}_{0.07})\Sigma_{3.00}^{\text{W}}(\text{F}_{0.60}\text{O}_{0.40})\Sigma_{1.00}$
Blue-green intermediate zone (I2)	$^{\text{X}}(\text{Na}_{0.50}\square_{0.24}\text{Ca}_{0.26})\Sigma_{1.00}^{\text{Y}}(\text{Al}_{1.39}\text{Li}_{1.32}\text{Mn}_{0.20}^{2+}\text{Cu}_{0.01})\Sigma_{2.91}^{\text{Z}}\text{Al}_6(\text{Si}_{6.09}\text{O}_{18})(\text{BO}_3)_3^{\text{V}}(\text{OH})_{3.00}^{\text{W}}(\text{OH}_{0.12}\text{F}_{0.57}\text{O}_{0.31})\Sigma_{1.00}$
Purple intermediate zone (I3)	$^{\text{X}}(\text{Na}_{0.49}\square_{0.29}\text{Ca}_{0.22})\Sigma_{1.00}^{\text{Y}}(\text{Al}_{1.34}\text{Li}_{1.47}\text{Mn}_{0.07}^{2+}\text{Mn}_{0.01}^{2+}\text{Cu}_{0.01})\Sigma_{2.90}^{\text{Z}}\text{Al}_6(\text{Si}_{6.18}\text{O}_{18})(\text{BO}_3)_3^{\text{V}}(\text{OH})_{3.00}^{\text{W}}(\text{OH}_{0.04}\text{F}_{0.57}\text{O}_{0.39})\Sigma_{1.00}$
Dark-green prismatic overgrowth (R)	$^{\text{X}}(\text{Na}_{0.29}\square_{0.03}\text{Ca}_{0.68})\Sigma_{1.00}^{\text{Y}}(\text{Al}_{0.89}\text{Li}_{1.51}\text{Fe}_{0.18}^{2+}\text{Fe}_{0.01}^{3+}\text{Mn}_{0.15}^{2+}\text{Mg}_{0.05}\text{Ti}_{0.01})\Sigma_{2.80}^{\text{Z}}\text{Al}_6(\text{Si}_{6.19}\text{O}_{18})(\text{BO}_3)_3^{\text{V}}(\text{OH})_{3.00}^{\text{W}}(\text{OH}_{0.26}\text{F}_{0.74})\Sigma_{1.00}$

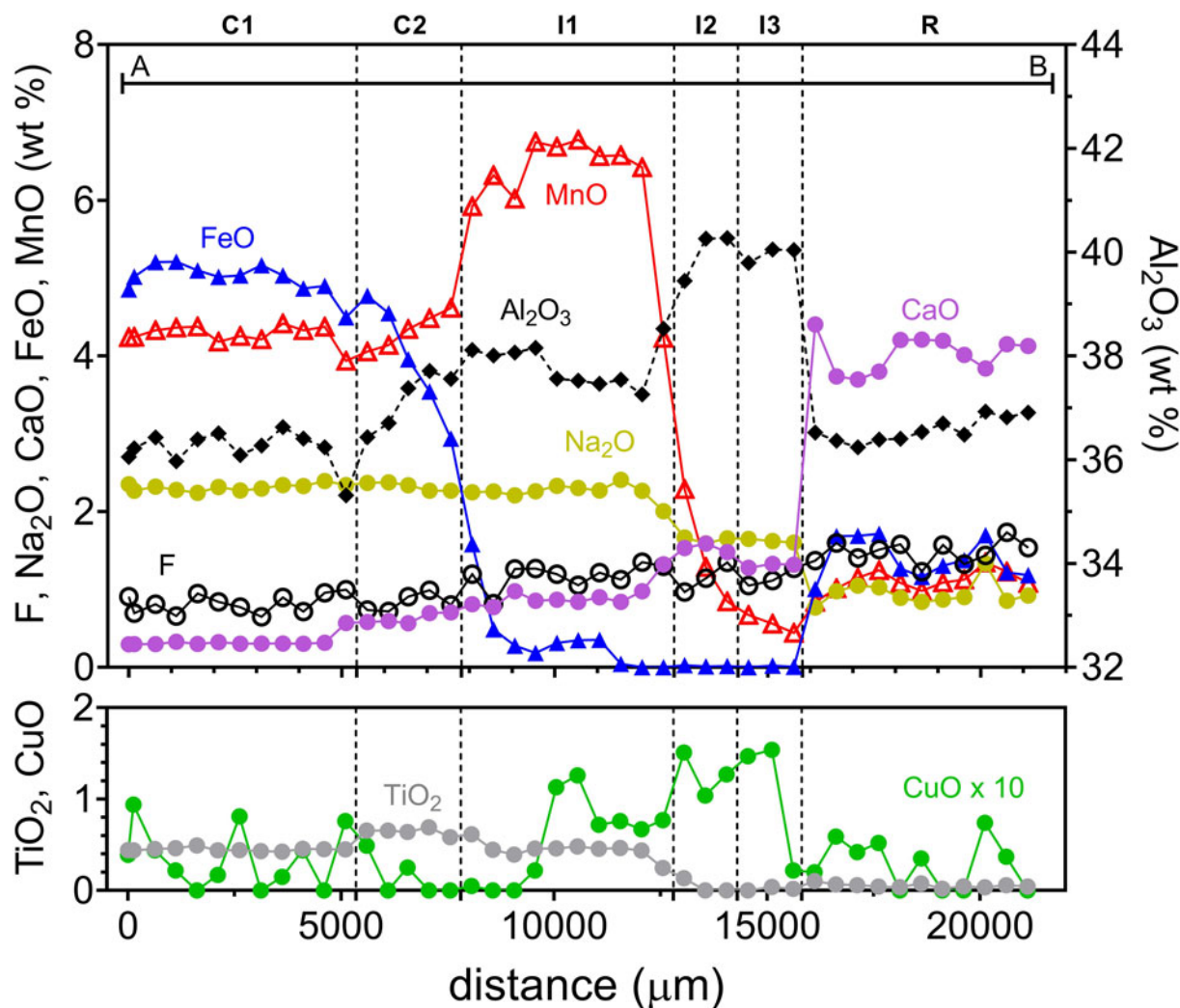


Figure 3. Results from EMPA of the tourmaline sample (only selected oxides are reported). See Table 1 for complete composition.

The outer part of the black core (C2) can be classified as a tourmaline belonging to the alkali-group, subgroup 4 (Henry *et al.*, 2011): it is Na-dominant at the X position of the tourmaline general formula and oxy-dominant at W with $O^{2-} > F^-$. Because it is ^ZAl - and $^Y(\text{Al}_2\text{Li})$ -dominant, its composition can be described as darrellhenryite, ideally $\text{Na}(\text{Al}_2\text{Li})\text{Al}_6(\text{Si}_6\text{O}_{18})(\text{BO}_3)_3(\text{OH})_3\text{O}$.

In contrast, the dark-green prismatic rim (R) can be classified as a tourmaline belonging to the calcic-group, subgroup 2 (Henry *et al.*, 2011): it is Ca-dominant at the X position and fluor-dominant at W with $(\text{OH}+\text{F})^- > O^{2-}$ and $F \gg (\text{OH})$. Because it is ^ZAl - and $^Y(\text{Li}_2\text{Al})$ -dominant, its composition is considered to be fluor-liddicoatite, ideally $\text{Ca}(\text{Li}_2\text{Al})\text{Al}_6(\text{Si}_6\text{O}_{18})(\text{BO}_3)_3(\text{OH})_3\text{F}$.

Discussion

Causes of colour

Colours in tourmaline are essentially related to the transition elements (Ti, V, Cr, Fe, Mn and Cu), acting as colour-causing agents through several mechanisms at structural levels, with the most common ones being crystal field transitions (CFT), intervalence charge transfer (IVCT) interactions, and colour centres (Fritsch and Rossman, 1987; Pezzotta and Laurs, 2011; Rossman, 2014).

Since compositional analyses of the different coloured zones did not reveal V_2O_3 and Cr_2O_3 (levels below the detection limit ≤ 0.03 wt.%), the main transition metals that could contribute to the colour of the tourmaline investigated are Fe, Mn, Ti and Cu.

The black colour characterising the core zone (C1, C2) hindered the recording of an optical absorption spectrum. Nevertheless, we can assess that such a colour is caused mainly by the highly absorbing Fe^{2+} transitions because of the abundance of this element in the inner core zone ($\text{FeO} > 4$ wt.%).

The spectrum of the yellow intermediate zone (I1) has a very strong absorption band in the near UV-region at ~ 30700 cm^{-1} and a sharp and very weak absorption band at ~ 24000 cm^{-1} , which can be assigned to $\text{Mn}^{2+}-\text{Ti}^{4+}$ IVCT and Mn^{2+} spin-forbidden transitions, respectively (Rossman and Mattson, 1986; da Fonseca-Zang *et al.*, 2008) (Fig. 5). This assignment is consistent with the enrichment in MnO and TiO_2 observed from compositional data (Table 4). Because the yellow coloration is mainly caused by an intervalence charge transfer $\text{Mn}^{2+}-\text{Ti}^{4+}$ interaction and to a minor extent by Mn^{2+} spin-forbidden transition, the I1 zone corresponds to the ‘canary’ tourmaline gemmological variety described in Laurs *et al.* (2007).

The spectrum recorded in the pale blue–green intermediate zone (I2) reveals only the presence of a very weak broad band

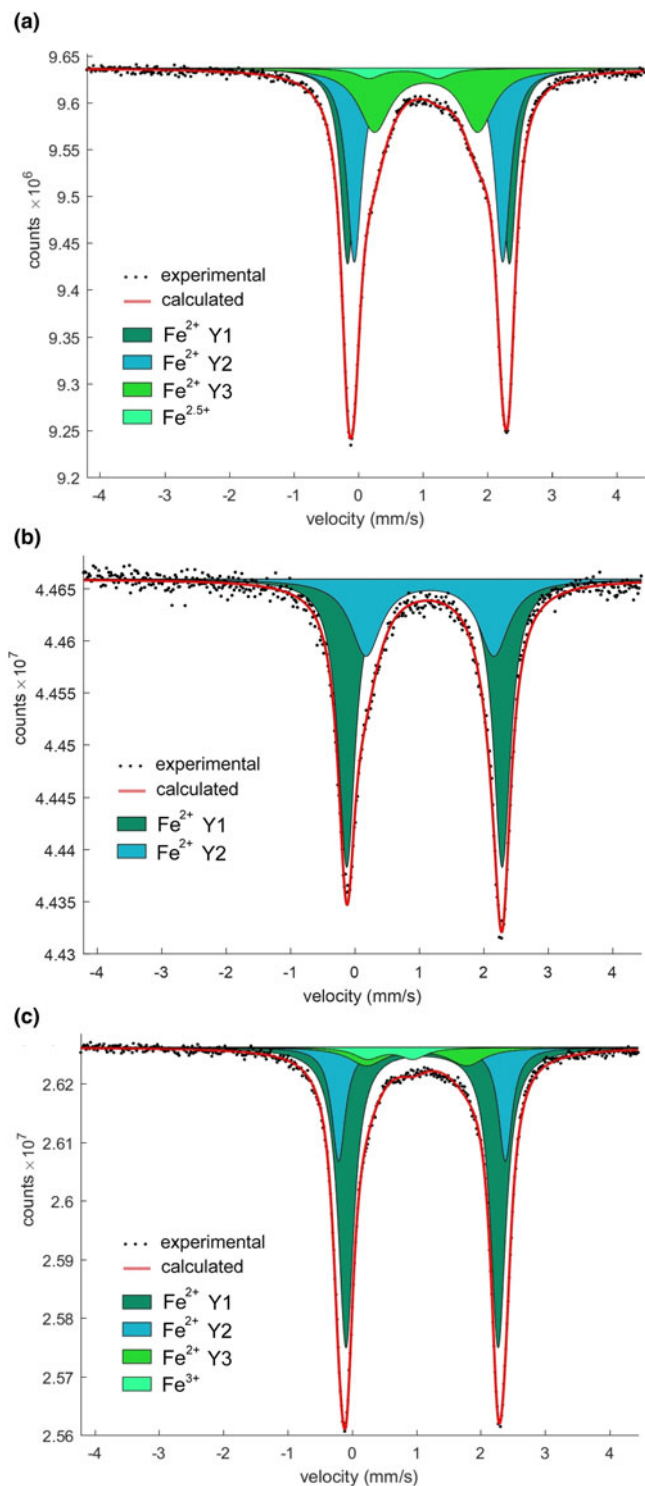


Figure 4. Room-temperature ^{57}Fe Mössbauer spectra for the black core (C1, C2), the yellow intermediate zone (I1) and the dark-green prismatic rim (R). For all the coloured zones (a, b, c), the experimental spectrum is represented by dots, and the calculated spectrum by a thick red curve. Lorentzian absorption doublets assigned to $^{61}\text{Fe}^{2+}$ are represented by dark-green, light-blue and light-green coloured areas. The neon-green coloured area refers to the assignment of $^{61}\text{Fe}^{2.5+}$ and $^{61}\text{Fe}^{3+}$.

at $\sim 14000\text{ cm}^{-1}$ and an intense broad band at $\sim 11000\text{ cm}^{-1}$ in the near-infrared-range, both ascribed to Cu^{2+} spin-allowed d - d transitions (Rossman *et al.*, 1991; Mashkovtsev *et al.*, 2006) (Fig. 5). Results from EPMA confirmed the enrichment in Cu

in this part of the crystal, with an amount up to double than that of the yellow zone (Fig. 3). This fits well with the different intensity of the absorption bands relative to Cu observed in the blue and the yellow zones. The relatively low MnO concentration ($< 2\text{ wt.}\%$) does not contribute to the colour through Mn^{2+} spin-forbidden electronic transitions, as Mn^{2+} is a weak absorber (Rossman, 2014). In addition, a lack of TiO_2 , prevents Mn–Ti interaction and consequently prevents the occurrence of a stronger Mn^{2+} – Ti^{4+} IVCT absorption band. Thus, in the absence of Fe (Table 4), Cu is the only colour-causing agent for the pale blue–green colouration of the I2 zone. Moreover, on the basis of overall results, the pale blue–green intermediate zone (I2) can be classified as the ‘Paraiba’ tourmaline variety (Laurs *et al.*, 2008).

The optical absorption spectrum of the purple intermediate zone (I3) is characterised by a weak and broad absorption band at $\sim 22000\text{ cm}^{-1}$ and a stronger broad band at $\sim 19000\text{ cm}^{-1}$, both ascribable to Mn^{3+} d - d transitions (Reinitz and Rossman, 1988; Taran *et al.*, 1993; Ertl *et al.*, 2005; Bosi *et al.*, 2017, 2021) (Fig. 5 and Table 4). These assignments agree with the purple colour of this part of the crystal, which can be ascribed to the presence of Mn^{3+} as a colour-causing agent. On the basis of the intensity of the band at $\sim 19000\text{ cm}^{-1}$ and using the molar extinction coefficient suggested by Reinitz and Rossman (1988), the Mn_2O_3 content was estimated to be 0.56 wt.% (Table 1) in the I3 zone. The origin of the broad and weak absorption bands at $\sim 25200\text{ cm}^{-1}$ and $\sim 14000\text{ cm}^{-1}$ is less obvious. The very low Fe and Ti content recorded by EMPA in this zone, rules out Fe^{2+} – Ti^{4+} IVCT as well as spin-allowed Fe^{2+} origins of these bands (Table 4). Other transition metals, such as Ni, can be taken into account (Taran *et al.*, 1993), although the absence of Ni in this sample rules out this possibility. Thus, the origin of these two absorption bands remains unclear. According to these data, the purple coloration of the I3 zone is dominated by the presence of Mn in the oxidised trivalent state. Nevertheless, the relatively significant content of Cu could add a minor bluish hue to the colour. Hence, this variety of Cu-bearing rubellite might correspond to the gemmological variety *cuprian-rubellite* (Fritsch *et al.*, 1990).

The spectrum of the dark-green prismatic overgrowth of the crystal displays two broad absorption bands centred at 13800 cm^{-1} and 9200 cm^{-1} , and a weak broad band at 24000 cm^{-1} , all attributable to the presence of relatively high levels of Fe (FeO up to 1.4 wt.%) (Fig. 5). Mössbauer analysis also shows, in addition to Fe^{3+} , the presence of Fe^{2+} . Thus, the two strong bands at 13800 cm^{-1} and 9200 cm^{-1} could be caused by electronic exchange interactions between the $\text{Fe}^{2+}/\text{Fe}^{3+}$ pair at adjacent Y sites in the tourmaline structure (Taran and Rossman, 2002) (Table 4). The set of weak and relatively sharp bands between ~ 25000 – 24000 cm^{-1} can instead be assigned to spin-forbidden Fe^{2+} and/or Fe^{3+} bands (Mattson and Rossman, 1987) (Table 4). In accord with these assignments, the dark-green colouration of the overgrowth is controlled mainly by $\text{Fe}^{2+}/\text{Fe}^{3+}$ interactions.

Growth history

The tourmaline sample analysed is composed of a relatively large detrital fragment, representing (from core-to-rim) all the growth sectors of an original crystal. Although there is no direct information regarding the primary deposit in which the original crystal formed, the changes of the composition observed in the sample allows some significant inferences concerning the original growth

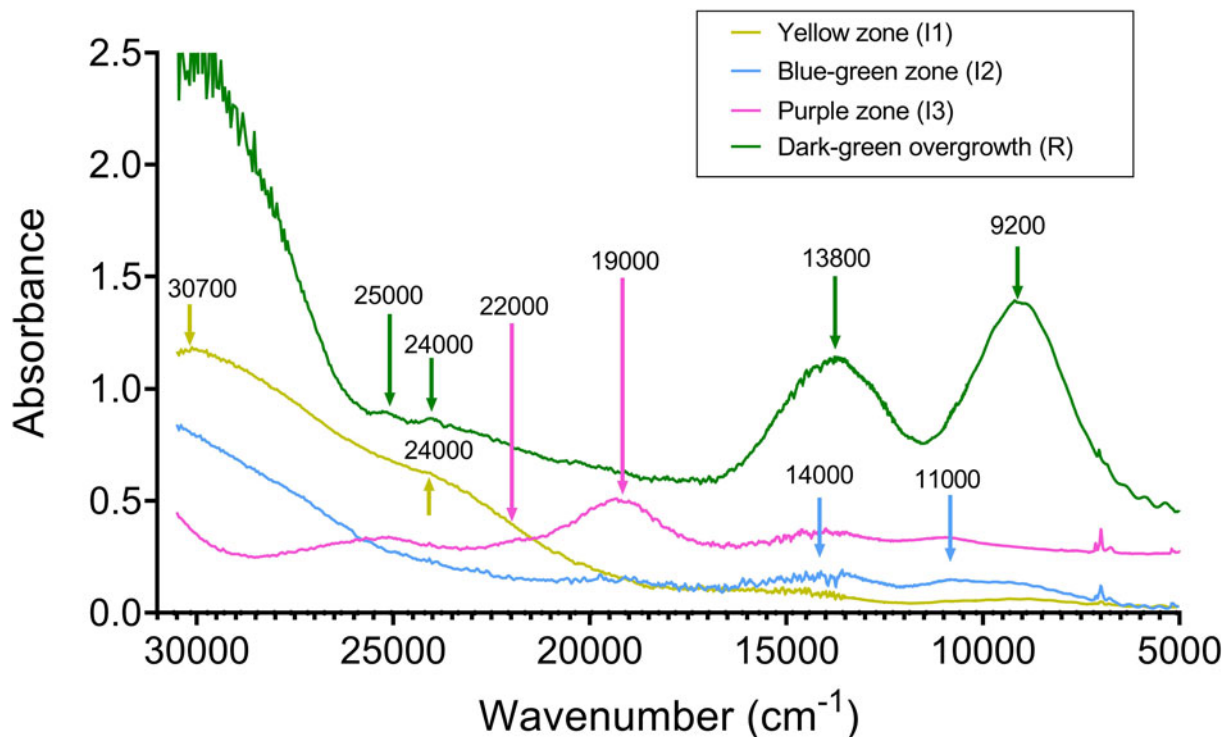


Figure 5. Optical absorption spectra for the different coloured zones of the tourmaline sample analysed. Sample thickness: yellow intermediate zone = 280 μm ; pale blue-green intermediate zone = 838 μm ; purple intermediate zone = 843 μm ; dark-green overgrowth = 424 μm . The main absorption bands are indicated.

stages, as well as the characteristics and the evolution of the crystallisation fluids.

The secondary Mavuco tourmaline deposit, from which the sample was collected, is located in the Alto Ligoña pegmatitic district characterised by a crystalline basement of amphibolitic facies with migmatitic domes, into which a number of gem-bearing LCT pegmatites of the upper Neoproterozoic age have been intruded (Pinna *et al.*, 1993; Bettencourt Dias and Wilson, 2000; Lächelt, 2004). The main features of the sample investigated, in addition to the minerals associated with tourmaline as residual grains in the secondary Mavuco deposit, clearly indicate a pegmatitic origin for the primary deposit. Thus, it represents, from core-to-rim, the stages of growth of an original tourmaline crystal of pegmatitic origin. Moreover, the relatively high gemmological quality and geochemical evolution of this tourmaline indicates that the original crystal formed in the core zone of a pegmatitic vein, very probably, in a miarolitic cavity.

The black inner core of the crystal exhibits a significant enrichment in Fe and Mn (FeO > 5 wt.% and MnO > 4 wt.%). This enrichment is related to the amount of these elements available in the pegmatitic system during the early crystallisation of tourmaline. The subsequent progressive decrease in Fe, with FeO contents decreasing to below the detection limit in the outermost part of the core zone, and remaining close to zero in the intermediate zone, is the result of Fe-depletion in the system, due mostly to tourmaline crystallisation. Indeed, MnO, shows an increase up to over 6 wt.% in the intermediate zone, then falling in the outermost intermediate zone to very low values (< 0.5 wt.%). The increased incorporation of Mn that characterises the yellow intermediate zone (I1) could be promoted by the depletion of Fe in the pegmatitic melt. In fact, the MnO content in the tourmaline crystal rises when the FeO content starts to decrease (Fig. 3), and this profile could be related to the behaviour of Mn during pegmatite crystallisation. Manganese is incompatible in typical magmatic

Table 4. Interpretation of OAS results for selected spot analyses on different coloured zones in the tourmaline sample investigated.

Colour	FeO (wt.%)	MnO (wt.%)	TiO ₂ (wt.%)	CuO (wt.%)	Absorption bands	Assignments
Yellow intermediate zone (I1)	–	6.42	0.44	0.07	~30700 cm ⁻¹ ~24000 cm ⁻¹	Mn ²⁺ –Ti ⁴⁺ IVCT transitions Mn ²⁺ spin-forbidden transitions
Blue-green intermediate zone (I2)	0.02	1.47	0.04	0.13	~14000 cm ⁻¹ ~11000 cm ⁻¹	Cu ²⁺ <i>d-d</i> transitions Cu ²⁺ <i>d-d</i> transitions
Purple intermediate zone (I3)	0.01	0.56	0.02	0.02	~22000 cm ⁻¹ ~19000 cm ⁻¹	Mn ³⁺ <i>d-d</i> transitions Mn ³⁺ <i>d-d</i> transitions
Dark-green prismatic overgrowth (R)	1.37	1.20	0.05	0.03	~25000 cm ⁻¹ ~24000 cm ⁻¹ ~13800 cm ⁻¹ ~9200 cm ⁻¹	Fe ²⁺ and/or Fe ³⁺ spin-forbidden transitions Fe ²⁺ and/or Fe ³⁺ spin-forbidden transitions Fe ³⁺ –Fe ²⁺ exchange-coupled pairs Fe ³⁺ –Fe ²⁺ exchange-coupled pairs

primitive tourmaline (schorl–foitite), whereas Fe is very compatible, and thus the progressive increase in the Mn/Fe ratio of melt is driven by the crystallisation of tourmaline (London *et al.*, 2001; Maner *et al.*, 2019).

However, during the latest stages of growth of the crystal, a sharp, new increase in Fe and Mn occurred, as documented by the dark-coloured prismatic overgrowth. A similar phenomenon has been described in the tourmaline crystals from Elba Island (Italy). These crystals are typically characterised by a sudden late-stage Fe and/or Mn enrichment, which results in dark-coloured overgrowths, mostly evident at the termination of the crystals (Pezzotta, 2021; Altieri, 2023; Altieri *et al.*, 2022, 2023a, 2023b). As has been argued for the Elba Island tourmalines petrogenetic model, a pocket rupture event related to brittle deformations occurring during the latest stages of crystallisation of the cavities in the pegmatitic rock, was responsible for a partial opening of the geochemical system. According to this model, the highly reactive late-stage cavity fluids were able to penetrate the fractures in the pegmatitic rock around the cavity. Consequently, this led to the hydrothermal alteration of the early-crystallised Fe- and Mn-rich minerals, such as Fe-rich micas and almandine–spessartine garnet. The release of Fe and Mn in the system caused a dramatic change in the composition of the pocket environment with the subsequent formation of the dark-coloured overgrowth. The observed significant increase in Ca in the dark-coloured tourmaline overgrowth might be related to two potential factors. Firstly, it could be linked to the destabilisation of early crystallised plagioclase crystals in the pegmatitic rock. Alternatively, it could be the result of fluid contamination originating from the metamorphic crystalline rocks into which the pegmatite was emplaced.

The CuO content is always low, with the highest values (~0.15 wt.%) in the I2 and the I3 zones. It is noteworthy that the highest values correspond to geochemically evolved growth sectors (Fig. 3). The occurrence of Cu in pegmatitic systems is interpreted as a contamination of the pegmatitic liquids/fluids, which could have occurred at the source or even at the emplacement level (e.g. Beurlen *et al.*, 2011; Beckett-Brown *et al.*, 2023). However, the profile of the abundance of Cu in tourmaline crystals growth is still poorly documented.

The presence of Mn³⁺ in the I3 zone, which results in the pink–red colouration, could suggest a change towards oxidising conditions in the environment. This contrasts with the very low oxidising conditions in which the tourmaline crystallised. In fact, Mössbauer data show an Fe³⁺/Fe_{tot} ratio of 0.02 in the core zone, the presence of only Fe²⁺ in the yellow intermediate zone (I1), and a Fe³⁺/Fe_{tot} ratio of 0.04 that characterises the dark-green prismatic overgrowth. In this particular scenario, it proves challenging to elucidate the sudden and temporary transition to oxidised conditions in the environment during crystallisation of the observed pink–red I3 zone. The possibility of a geochemical system opening at this stage can be ruled out because no sudden changes in the composition can be observed in the I3 zone. A possible explanation for the occurrence of Mn³⁺ in the I3 zone can be ascribed to the presence of a low amount of Mn³⁺ in the original melt. It has been reported that the Mn partition coefficient is anomalously low for Mn³⁺ and Mn uptake by tourmaline is dominated by Mn²⁺ (van Hinsberg, 2011). Thus, the Mn³⁺/Mn²⁺ ratio increased as consequence of the preferential incorporation of Mn²⁺ by tourmaline and the incorporation of Mn³⁺ occurred once Mn²⁺ had been completely depleted. Another explanation to account for the change in the redox state which occurred in the

pink–red I3 zone, where Mn³⁺ prevails, is to assume that tourmaline, after crystallisation, encountered a natural radiation source, thereby inducing the Mn²⁺ oxidation and consequently leaving an overprint in the composition. However, the oxidising effects of any radiation source only become evident in the I3 zone, characterised by the lowest Mn content and absence of Fe. We suggest that, in addition to other phenomena, the Mn²⁺ and Ti⁴⁺ IVCT interaction might offer a stabilising effect against the oxidation of Mn. According to this, the initial part of the crystal, up to the yellow intermediate zone (I1), is enriched in TiO₂ (> 0.4 wt.%) and MnO (> 1.5 wt.%), whereas TiO₂ is undetectable in the pink–red I3 zone. To the best of our knowledge, this explanation has not been proposed previously in the literature. It introduces a new concept that has the potential to open up a new area of research.

Conclusions

This work investigated a fragment of a multicoloured tourmaline from the secondary deposit of Mavuco (Alto Ligoña, Mozambique), which represents the growth history from core-to-rim of the original crystal. By combining data obtained by compositional and spectroscopic investigations, it was possible to determine the colour-causing agents that characterise the different coloured zones of the crystal.

The polychromatic feature of this tourmaline fragment highlights the petrogenetic potential of tourmaline as a powerful tool to register physicochemical variation in the crystallisation environment. However, the presence of a change in the redox state of Mn within a limited zone, probably occurred after the tourmaline crystallisation, and might represent evidence of post-crystallisation alteration of the compositional signature of the tourmaline crystal.

Acknowledgements. Sample preparation for compositional and spectroscopic analyses was carried out with the support of Dr. D. Mannetta to whom the authors express their gratitude. The authors sincerely thank M. Serracino for his assistance during chemical analyses. The company Mozambique Mining is acknowledged for providing the studied sample. The authors sincerely thank the reviewers Peter Bačik and Andreas Ertl for their constructive comments that helped to improve the manuscript. This research received funding by Sapienza University of Rome (Prog. Università 2023 to F.B.)

Author contributions. F.P. and F.B. conceived the project. F.B. created the working group. F.P. selected the research material and collected the field information. A.A. and F.B. provided EMPA data. H.S. and U.H. provided MS and OAS data. A.A. analysed the data and wrote the first draft of the manuscript. F.P. contributed to the discussion section. All the authors reviewed the final version of the manuscript.

Competing interests. The authors declare none.

References

- Altieri A. (2023) Definition of a genetic model for the dark-colored overgrowths in pegmatitic gem tourmaline crystals. *Plinius*, **49**, 23–29.
- Altieri A., Pezzotta F., Skogby H., Hälenius U. and Bosi F. (2022) Blue-growth zones caused by Fe²⁺ in tourmaline crystals from the San Piero in Campo gem-bearing pegmatites, Elba Island, Italy. *Mineralogical Magazine*, **86**, 910–919.
- Altieri A., Pezzotta F., Skogby H., Hälenius U. and Bosi F. (2023a) Dark-coloured Mn-rich overgrowths in an elbaite tourmaline crystal from the Rosina pegmatite, San Piero in Campo, Elba Island, Italy: witness of late-stage opening of the geochemical system. *Mineralogical Magazine*, **87**, 130–142.

- Altieri A., Pezzotta F., Andreozzi G.B., Skogby H., and Bosi F. (2023b) Genetic model for the color anomalies at the termination of pegmatitic gem tourmaline crystals from the island of Elba, Italy. *European Journal of Mineralogy*, **35**, 755–771.
- Andreozzi G.B., Bosi F. and Longo M. (2008) Linking Mossbauer and structural parameters in elbaite-schorl-dravite tourmalines. *American Mineralogist*, **93**, 658–666.
- Beckett-Brown C., McDonald A.M. and McClenaghan M.B. (2023) Trace element characteristics of tourmaline in porphyry Cu systems: development and application to discrimination. *The Canadian Journal of Mineralogy and Petrology*, **61**, 31–60.
- Bettencourt Dias M., Wilson W.E. (2000) Famous mineral localities: The Alto Ligonha pegmatites, Mozambique. *Mineralogical Record*, **31**, pp. 459–497.
- Beurlen H., De Moura O.J.M., Soares D.R., Da Silva M.R.R. and Rhede D. (2011) Geochemical and geological controls on the genesis of gem-quality “Paraíba Tourmaline” in granitic pegmatites from northeastern Brazil. *The Canadian Mineralogist*, **49**, 277–300.
- Bosi F., Cámara F., Ciriotti M.E., Hålenius U., Reznitskii L. and Stagno V. (2017) Crystal-chemical relations and classification problems of tourmalines belonging to the oxy-schorl–oxy-dravite–bosiite–povondraite series. *European Journal of Mineralogy*, **29**, 445–455.
- Bosi F., Celata B., Skogby H., Hålenius U., Tempesta G., Ciriotti M.E., Bittarello E. and Marengo A. (2021) Mn-bearing purplish-red tourmaline from the Anjanaboina pegmatite, Madagascar. *Mineralogical Magazine*, **85**, 242–253.
- Bosi F., Pezzotta F., Altieri A., Andreozzi G.B., Ballirano P., Tempesta G., Cempírek J., Škoda R., Filip J., Čopjácová R., Novák M., Kampf A.R., Scribner E.D., Groat L.A. and Evans, R.J. (2022) Celleriite, $\square(\text{Mn}_2^+ \text{Al})\text{Al}_6(\text{Si}_6\text{O}_{18})(\text{BO}_3)_3(\text{OH})_3(\text{OH})$, a new mineral species of the tourmaline supergroup. *American Mineralogist*, **107**, 31–42.
- da Fonseca-Zang W.A., Zang J.W. and Hofmeister W. (2008) The Ti-influence on the tourmaline color. *Journal of the Brazilian Chemical Society*, **19**, 1186–1192.
- Dutrow B.L. and Henry D.J. (2011) Tourmaline: A geologic DVD. *Elements*, **7**, 301–306.
- Dutrow B.L. and Henry D.J. (2018) Tourmaline compositions and textures: reflections of the fluid phase. *Journal of Geosciences*, **63**, 99–110.
- Ertl A., Rossman G.R., Hughes J.M., Prowatke S. and Ludwig T. (2005) Mn-bearing “oxy-rossmanite” with tetrahedrally coordinated Al and B from Austria: Structure, chemistry and infrared and optical spectroscopic study. *American Mineralogist*, **90**, 481–487.
- Ertl A., Marschall H.R., Giester G., Henry D.J., Schertl H.-P., Ntaflou T., Luvizotto G.L., Nasdala L., and Tillmanns E. (2010) Metamorphic ultra high-pressure tourmalines: Structure, chemistry, and correlations to PT conditions. *American Mineralogist*, **95**, 1–10.
- Ertl A., Giester G., Schüssler U., Brätz H., Okrusch M., Tillmanns E. and Bank H. (2013) Cu- and Mn-bearing tourmalines from Brazil and Mozambique: crystal structures, chemistry and correlations. *Mineralogy and Petrology*, **107**, 265–279.
- Fritsch E. and Rossman G.R. (1987) An update on color in gems. Part I. Introduction and colors caused by dispersed metal ions. *Gems and Gemology*, **23**, 126–139.
- Fritsch E., Shigley J.E., Rossman G.R., Mercer M.E., Muhlmeister S.M. and Moon M. (1990) Gem-quality cuprian-elbaite tourmalines from São José da Batalha, Paraíba, Brazil. *Gems and Gemology*, **26**, 189–205.
- Henry D.J. and Dutrow B.L. (2018) Tourmaline studies through time: contributions to scientific advancements. *Journal of Geosciences*, **63**, 77–98.
- Henry D.J., Novák M., Hawthorne F.C., Ertl A., Dutrow B., Uher P. and Pezzotta F. (2011) Nomenclature of the tourmaline supergroup minerals. *American Mineralogist*, **96**, 895–913.
- Lächelt S. (2004) *The Geology and Mineral Resources of Mozambique*. National Directorate of Geology, Maputo, Mozambique, 515 pp.
- Laurs B.M., Simmons W.B., Rossman G.R., Fritz E.A., Koivula J.I., Ankar B. and Falster A.U. (2007) Yellow Mn-rich tourmaline from the Canary Mining Area, Zambia. *Gems & Gemology*, **43**, 314–331.
- Laurs B.M., Zwaan J.C., Breeding C.M., Simmons W.B., Beaton D., Rijdsdijk K.F., Befi R. and Falster A.U. (2008) Copper-bearing (Paraíba-type) tourmaline from Mozambique. *Gems & Gemology*, **44**, 4–30.
- London D., Evensen J.M., Fritz E.A., Icenhower J.P., Morgan G.B. and Wolf M.B. (2001) Enrichment and accommodation of manganese in granite-pegmatite systems. *Eleventh Annual V.M. Goldschmidt Conference*, Abstract #3369 (Lunar and Planetary Institute, Houston)
- Maner IV J.L., London D. and Icenhower J.P. (2019) Enrichment of manganese to spessartine saturation in granite-pegmatite systems. *American Mineralogist*, **104**, 625–1637.
- Mashkovtsev R.I., Smirnov S.Z. and Shigley J.E. (2006) The features of the Cu²⁺-entry into the structure of tourmaline. *Journal of Structural Chemistry*, **42**, 252–257.
- Mattson S.M. and Rossman G.R. (1987) Fe²⁺-Fe³⁺ interactions in tourmaline. *Physics and Chemistry of Minerals*, **14**, 163–171.
- Okrusch M., Ertl A., Schüssler U., Tillmanns E., Brätz H. and Bank H. (2016) Major- and trace-element composition of Paraíba-type Tourmaline from Brazil, Mozambique and Nigeria. *Journal of Gemmology*, **35**, 120–139.
- Pesquera A., Gil-Crespo P.P., Torres-Ruiz F., Torres-Ruiz J. and Roda-Robles E. (2016) A multiple regression method for estimating Li in tourmaline from electron microprobe analyses. *Mineralogical Magazine*, **80**, 1129–1133.
- Pezzotta F. (2021) A history of tourmaline from the Island of Elba. *The Mineralogical Record*, **52**, 669–720.
- Pezzotta F. and Laurs B.M. (2011) Tourmaline: The kaleidoscopic gemstone. *Elements*, **7**, 331–336.
- Pinna P., Jourde G., Calvez J.Y., Mroz J.P., Marques J.M. (1993) The Mozambique Belt in northern Mozambique: Neo-proterozoic (1100–850 Ma) crustal growth and tectogenesis, and superimposed Pan-African (800–550 Ma) tectonism. *Precambrian Research*, **62**, pp. 1–59.
- Pouchou J.L. and Pichoir F. (1991) Quantitative analysis of homogeneous or stratified microvolumes applying the model “PAP”. Pp. 31–75 in: *Electron Probe Quantitation* (K.F.J. Heinrich and D.E. Newbury, editors). Plenum, New York.
- Prescher C., McCammon C. and Dubrowsky L. (2012) MossA: a program for analyzing energy-domain Mössbauer spectra from conventional and synchrotron sources. *Journal of Applied Crystallography*, **45**, 329–331.
- Reinitz I. and Rossman G.R. (1988) Role of natural radiation in tourmaline coloration. *American Mineralogist*, **73**, 822–825.
- Rossman G.R. (2014) Optical spectroscopy. Pp. 371–398 in: *Spectroscopic Methods in Mineralogy and Materials Sciences* (G.S. Henderson, D.R. Neuville and R.T. Downs, editors). Reviews in Mineralogy and Geochemistry, **78**. Mineralogical Society of America, Chantilly, Virginia, USA.
- Rossman G.R. and Mattson S.M. (1986) Yellow, Mn-rich elbaite with Mn-Ti intervalence charge transfer. *American Mineralogist*, **71**, 599–602.
- Rossman G.R., Fritsch E. and Shigley J.E. (1991) Origin of color in cuprian elbaite from São José de Batalha, Paraíba, Brazil. *American Mineralogist*, **76**, 1479–1484.
- Taran M.N. and Rossman G.R. (2002) High-temperature, high-pressure optical spectroscopic study of ferric-iron-bearing tourmaline. *American Mineralogist*, **87**, 1148–1153.
- Taran M.N., Lebedev A.S. and Platonov A.N. (1993) Optical absorption spectroscopy of synthetic tourmalines. *Physics and Chemistry of Minerals*, **20**, 209–220.
- van Hinsberg V.J. (2011) Preliminary experimental data on trace-element partitioning between tourmaline and silicate melt. *The Canadian Mineralogist*, **49**, 153–163.
- van Hinsberg V.J., Henry D.J. and Dutrow B.L. (2011a) Tourmaline as a petrologic forensic mineral: A unique recorder of its geologic past. *Elements*, **7**, 327–332.
- van Hinsberg V.J., Henry D.J. and Marschall H.R. (2011b) Tourmaline: an ideal indicator of its host environment. *The Canadian Mineralogist*, **49**, 1–16.